



Measurements of Seismic Anisotropy in Synthetic Rocks with Controlled Crack Geometry and Different Crack Densities

PINBO DING,^{1,2,4} BANGRANG DI,^{1,2} DING WANG,³ JIANXIN WEI,^{1,2} and XIANGYANG LI^{1,2,4}

Abstract—Seismic anisotropy can help to extract azimuthal information for predicting crack alignment, but the accurate evaluation of cracked reservoir requires knowledge of degree of crack development, which is achieved through determining the crack density from seismic or VSP data. In this research we study the dependence of seismic anisotropy on crack density, using synthetic rocks with controlled crack geometries. A set of four synthetic rocks containing different crack densities is used in laboratory measurements. The crack thickness is 0.06 mm and the crack diameter is 3 mm in all the cracked rocks, while the crack densities are 0.00, 0.0243, 0.0486, and 0.0729. P and S wave velocities are measured by an ultrasonic investigation system at 0.5 MHz while the rocks are saturated with water. The measurements show the impact of crack density on the P and S wave velocities. Our results are compared to the theoretical prediction of Chapman (J App Geophys 54:191–202, 2003) and Hudson (Geophys J R Astron Soc 64:133–150, 1981). The comparison shows that measured velocities and theoretical results are in good quantitative agreement in all three cracked rocks, although Chapman’s model fits the experimental results better. The measured anisotropy of the P and S wave in the four synthetic rocks shows that seismic anisotropy is directly proportional to increasing crack density, as predicted by several theoretical models. The laboratory measurements indicate that it would be effective to use seismic anisotropy to determine the crack density and estimate the intensity of crack density in seismology and seismic exploration.

Key words: Seismic anisotropy, crack density, synthetic rock, equivalent medium theory.

1. Introduction

A medium whose physical properties are function of spatial orientation is said to be anisotropic. Seismic waves propagating in anisotropic rocks travel at different velocities depending on the direction of propagation and polarization. Due to recent developments in long offset, wide azimuthal and high-quality multicomponent acquisition, anisotropy is increasingly applied to pre-stack depth migration, parameter estimation, and other seismic processing and inversion techniques involving anisotropic models. Seismic anisotropy, defined as seismic wave velocity variation with propagation or polarization direction, can be caused by mineral alignment (Sarout and Guéguen 2008a, b; Sarout et al. 2007; Valcke et al. 2006; Vernik and Nur 1992), layering (Backus 1962), grain scale fabrics (Hall et al. 2008), and especially cracks (Crampin 1984; Guéguen and Sarout 2009, 2011; Hudson 1981; Thomsen 1995). Cracks aligned in a preferential direction which is controlled by the in situ stress field can make rocks strongly anisotropic at the seismic scale (Chapman et al. 2002; Zatsepin and Crampin 1997).

Seismic anisotropy can be expressed in terms of Thomsen’s anisotropy parameters which are a simple and convenient way to describe the strength of anisotropy in a transversely isotropic medium (Thomsen 1986). The P-wave anisotropy parameter, ε , describes the strength of P-wave velocity anisotropy. This parameter can be calculated from the elastic tensor stiffness components c_{ij} or by the difference in squared P-wave velocity for propagation in the directions parallel and perpendicular to the cracks:

$$\varepsilon = \frac{c_{11} - c_{33}}{2c_{33}}. \quad (1)$$

¹ State Key Laboratory of Petroleum Resource and Prospecting, China University of Petroleum (Beijing), Beijing 102249, China. E-mail: weijx@cup.edu.cn

² CNPC Key Laboratory of Geophysical Exploration, China University of Petroleum (Beijing), Beijing 102249, China.

³ Geophysical Research Institute, SINOPEC, Nanjing 211103, China.

⁴ Edinburgh Anisotropy Project, British Geological Survey, Edinburgh EH9 3LA, UK.

The S-wave anisotropy parameter γ describes the shear wave anisotropy calculated from elastic tensor or the SH wave velocity difference between polarizations parallel and perpendicular to the cracks:

$$\gamma = \frac{c_{66} - c_{44}}{2c_{44}}. \quad (2)$$

Seismic anisotropy caused by aligned cracks and influenced by crack geometry gives an effective method for determining the crack distribution and orientation in reservoir exploration, CO₂ storage, ground water flow, and hydraulic fracturing treatment. Anisotropy is directly influenced by the crack orientation, and thus provides azimuthal information to indicate crack alignment (Far et al. 2014). Azimuthal information extracted from seismic data (Boness and Zoback 2004; Lou et al. 1997) and VSP data (Kuwahara et al. 1991; Varghese et al. 2009) is used to investigate crack spatial orientation and density. The travel time and velocity information determined from wide azimuth seismic data can be used to estimate the crack orientation (Mallick and Frazer 1991; Wang 2011). However, more information on crack parameters, specifically crack density, is required in reservoir exploration and evaluation.

Schoenberg and Sayers (1995) presented a model which describes the crack-induced compliance tensor in terms of two crack compliances: the normal compliance Z_N and the tangential compliance Z_T . This model is used widely to invert for crack orientation from seismic data. Crack parameters were neglected in this model, particularly crack density, which is a key parameter for reservoir detection and production. The accurate estimation of crack density is still a challenge for geophysicists and reservoir engineers during geophysical prospecting and reservoir production.

The crack density was related to seismic anisotropy by the predictions of equivalent medium theories (Crampin 1984; Hudson 1981). The Hudson model provides a relationship between anisotropy and crack density, and shows that in cracked media the anisotropy is strongly dependent on crack density. The strength of seismic anisotropy due to aligned cracks is proportional to the crack density. Hudson's model assumes that the fluids are isolated in the cracks. This indicates that Hudson's model provides a

high-frequency limit. Chapman developed a multi-scale model to describe the frequency dependence of the elastic wave response for a medium containing heterogeneities of different scales (Chapman 2003; Chapman et al. 2002). The micro-scale pores and cracks cause squirt flow at higher frequencies, whilst the meso-scale fractures are responsible for wave-induced fluid flow which causes dispersion and attenuation at much lower frequencies. Thus the frequency dependence of the effective stiffness tensor is considered. In Chapman's model, crack density as well as pores and fluids is taken into account.

The crack density is defined by the number of cracks with a certain radius in a unit volume:

$$\varepsilon_c = \frac{N\alpha^3}{V}, \quad (3)$$

in which N is the number of aligned cracks of radius α , and V is the rock volume. The theoretical prediction requires experimental verification using rocks with known crack density. Unfortunately the crack parameters (crack geometry and density) are unknown in natural rocks; thus synthetic samples must be used in laboratory experiments to observe seismic wave propagation in cracked rocks. Ass' Ad et al. (1992) used sets of synthetic samples with cracks to observe shear wave anisotropy; their samples, constructed using epoxy and rubber, were different from natural rocks. Rathore et al. (1995) calibrated Thomsen model and Hudson model using synthetic sandstone bonded by epoxy. Rathore et al. (1995) presented P and S wave velocity results based on single synthetic sample, but did not provide the anisotropy comparison results. Rathore et al. (1995) also suggested that several samples should be tested for a complete study of elastic anisotropy in cracked media. Silicate cemented synthetic rocks were constructed to observe shear wave splitting (Tillotson et al. 2011, 2012), but the relationship of shear wave splitting to crack density was compared for only one cracked rock.

The aim of this study was to investigate velocity and anisotropy in cracked samples with different crack densities. We used a new construction method to build synthetic rocks which have similar mineral composition, porous structure, and cementation to natural rocks. A set of cracked rocks containing

controlled crack geometry and different crack density was used to observe the effects of seismic anisotropy. The changes of anisotropy caused by different crack densities were validated by the comparison between theoretical results and experimental data.

2. Methodology

In previous researches, synthetic cracked samples used materials such as lucite and silica rubber, which are different from natural rocks. Some samples used in previous works had no pores and crack spaces, and the cracks were represented by weak material (Ass' Ad et al. 1992; Cao et al. 2003; He et al. 2001; Wei et al. 2013). A new construction process has been used to build synthetic rocks which have similar mineral composition, pore structure, and cementation to natural rocks (Ding et al. 2013, 2014). We follow a typical manufacturing process in material science to build the synthetic rocks. This new process is more suitable for production of porous rocks with imbedded cracks (shown in Fig. 1). The materials we chose are silica sand and clay minerals, and sodium silicate

is used as a binder (shown in Fig. 2). The powder of silica sand and clays are mixed in ball mill for 24 h to ensure homogeneity and then mixed with sodium silicate. The mixture is then poured into a mold layer after layer. Pre-fabricated penny-shaped polymeric material discs are embedded in the synthetic samples through spread out over the surface of each layer. The mold is compressed under 10 MPa for 10 h, then is moved out and heated for 7 days at 80 °C. After the block has consolidated under these conditions, it is placed into a muffle oven and sintered in a high-temperature environment at 900 °C. The polymeric material discs decompose into gas and leak out the block under high temperature (above 900 °C), leaving penny-shaped cracks. Then the block is cut or cored into rock samples for laboratory experiments. The rock surface is then polished for better coupling with the ultrasonic transducers. Finally, the rock samples are dried and ready for laboratory testing and measurements. SEM (scanning electron microscope) is used to observe the porous structure (shown in Fig. 3) and X-ray CT is used to observe the crack shape and orientation (shown in Fig. 4).

In this study, a set of synthetic rocks with controlled crack density was built to investigate seismic anisotropy, and the crack density in three cracked rocks is 0.0243, 0.0486, and 0.0729, respectively. The crack diameter in all rock samples is 3 mm while the crack thickness is 0.06 mm. The size of each block is about 50 mm × 50 mm × 50 mm which are then grinded into octagonal prisms. The construction procedure and crack parameters for the three types of rocks are shown in Table 1. Figure 5 shows the final of synthetic rocks with controlled crack density. These synthetic rocks were immersed into water under vacuum extract air out ensure the rocks are optimally saturated with water. Then the water-saturated rocks were measured with an ultrasonic measurement system at 0.5 MHz, and the bulk modulus of the water is 2.19 GPa. The measurement error is about 0.8% for P wave velocity and 1.2% for S wave velocity. The P and SH (polarization in plane parallel to the cracks), and SV wave (polarization in plane perpendicular to cracks) were measured in directions 0° (perpendicular to cracks), 45°, 90° (parallel to cracks), and 135° (as shown in Fig. 5). During the experiments, SH waves were measured by

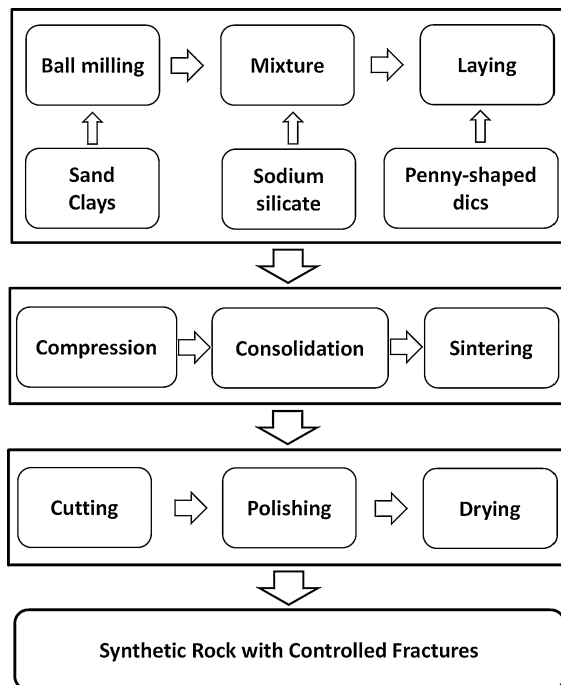


Figure 1

Construction process of synthetic rock with controlled cracks



Figure 2
Materials used to construct synthetic samples (silica sands, sodium silica and clays)

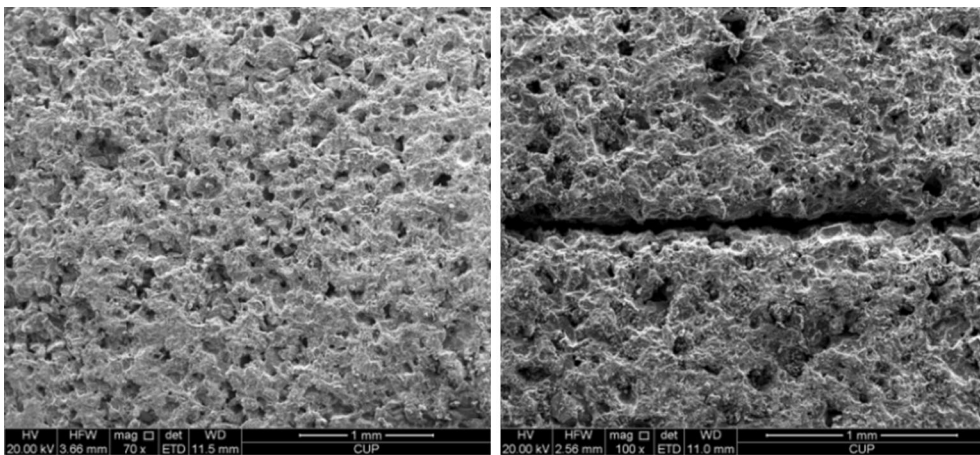


Figure 3
SEM images of pores and cracks in synthetic rock with controlled cracks

rotating the shear wave transducer until its polarization was parallel to the strike of the cracks, SV waves were measured by rotating the shear wave transducer until its polarization was perpendicular to the strike

of cracks. Figure 6 shows the P and S wave signal in different directions in four samples. Figure 6a–d shows the P wave transmission signal in blank sample with no cracks and samples with crack density of

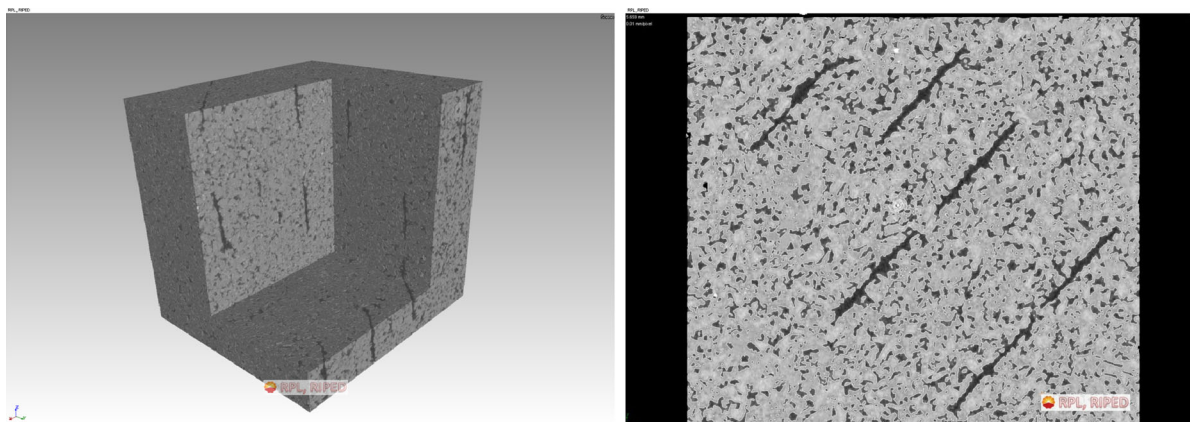


Figure 4
X-ray CT image of synthetic rock with controlled cracks

Table 1

Parameters of rocks and cracks

	1	2	3	4
Layer number	30	30	30	30
Number of discs/layer	0	30	60	90
Crack density	0	0.0243	0.0486	0.0729
Crack thickness	–	0.06 mm	0.06 mm	0.06 mm
Crack length	–	3 mm	3 mm	3 mm
Density	1.885 g/cc	1.883 g/cc	1.893 g/cc	1.870 g/cc
Frequency	0.5 MHz			
Fluid bulk modulus	2.19 GPa			
Fluid density	1.00 g/cc			
Fluid viscosity	1 cP			
Grain size	75 μ m			

0.0243, 0.0486, 0.0729, respectively. Figure 6b–d shows P waveforms in cracked samples change compared to P waveforms in blank sample (as shown in Fig. 6a), as well as the shear waveforms in Fig. 6f–h. These waveform changes reflect the interactions of the elastic wave signal with the cracks, similarly to what has been reported by Rathore et al. (1995). The main cause is the scattering (the wavelength is about 6.8 mm for P-wave and 4 mm for S-wave) of the stress wave with the cracks, especially in samples with high crack density (as shown in Fig. 6d, h).

3. Results

Figures 7, 8, 9, and 10 show the P and S wave velocities in different directions for the blank rock

and the three rocks containing controlled cracks with crack densities 0.0243, 0.0486, and 0.0729 (in water saturation, frequency is 0.5 MHz). Figure 7 shows the theoretical modeling results using Chapman (2003) and Hudson (1981) for the blank rock. Note that the blank rock exhibits some degree of anisotropy due to layer-by-layer deposition during the construction process. The model's prediction shown in Fig. 7 accounts for the background anisotropy (see Appendix). P-wave velocity in the 90° direction for three synthetic rocks with cracks in Figs. 8, 9 and 10 (i.e. parallel to cracks) decreases slightly as the crack density increases, compared to the blank rock (shown in Fig. 7). In contrast, the P-wave velocity in the 0° direction (i.e. perpendicular to cracks) decreases significantly in rocks containing higher crack density. S-wave velocities are significantly affected by crack

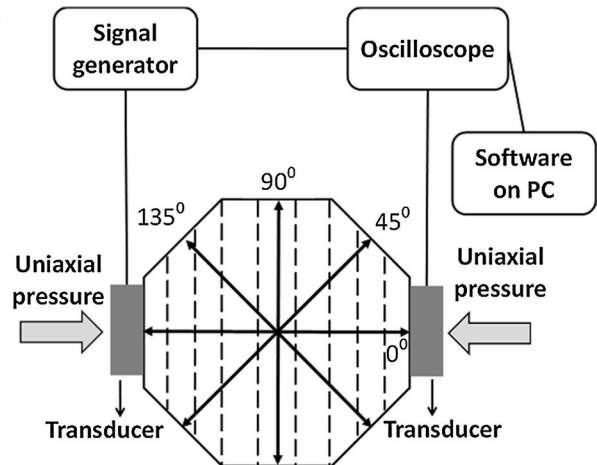
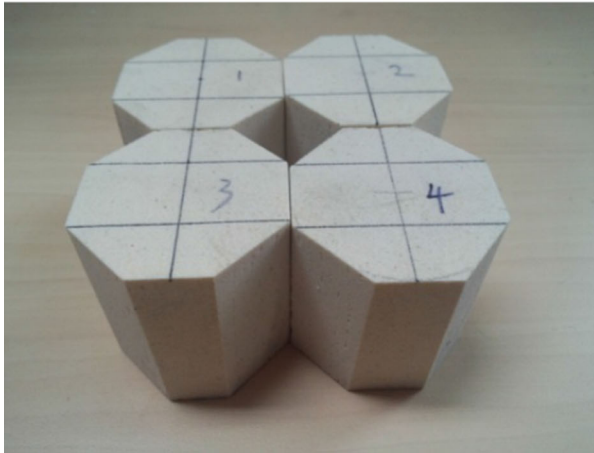


Figure 5

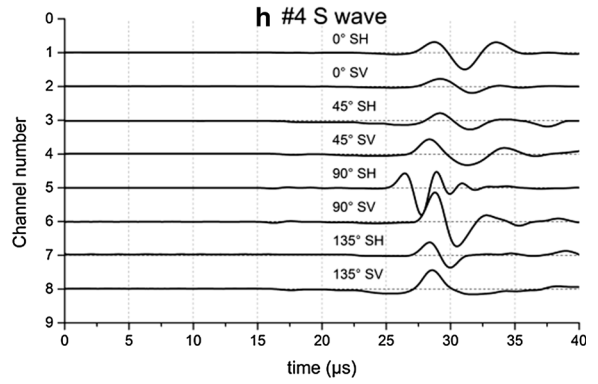
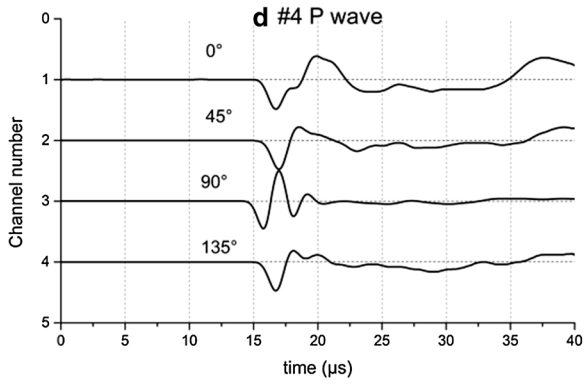
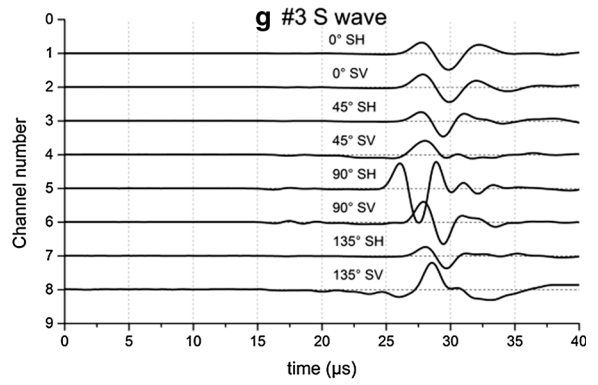
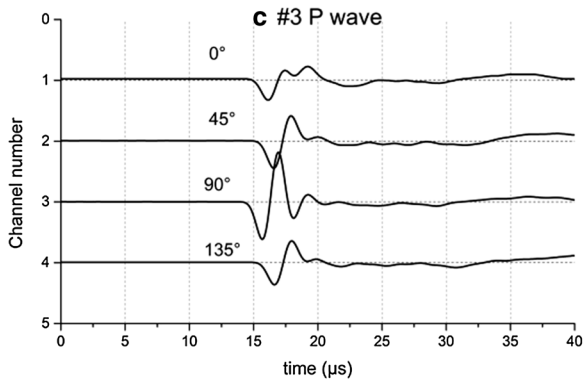
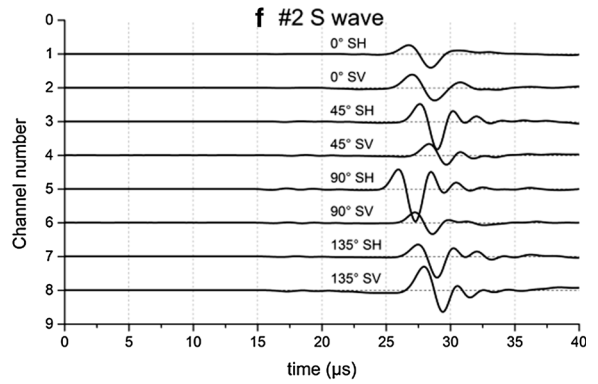
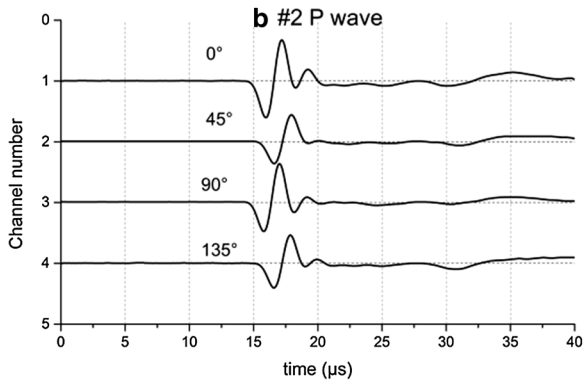
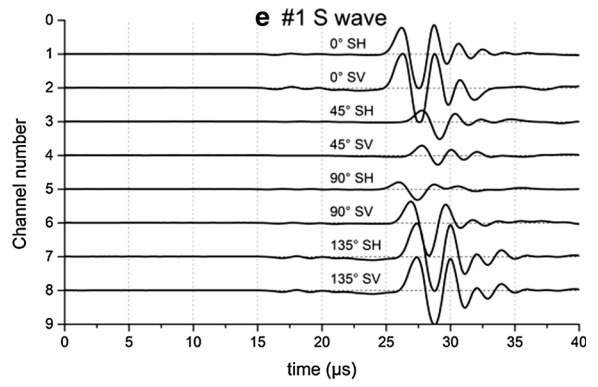
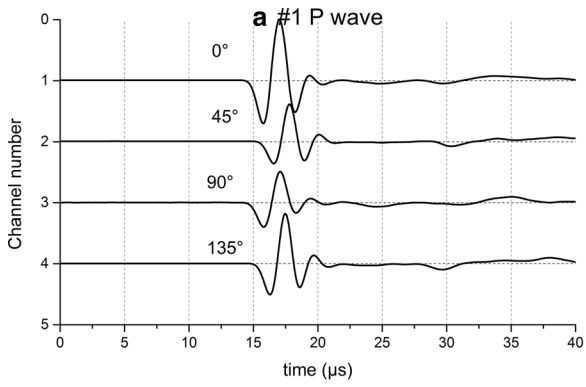
Synthetic rocks with controlled crack density (left) and the velocity measurements (right) (0° is the direction perpendicular to crack, also the isotropic symmetry axis; 90° is the direction parallel to cracks, also the crack plane direction)

density in the direction perpendicular to cracks. The shear wave velocity (for both SV wave and SH wave) in the 0° direction decreases as the crack density increases from 0.0243 to 0.0729. Moreover, crack density has a more substantial effect on the SV wave velocity than on the SH wave velocity, at 90° . The SV wave velocity decreases significantly compared to the SH wave velocity in the 90° direction (parallel to cracks). P- and SH waves show 2θ periodicity while the SV wave shows 4θ periodicity with the propagation direction.

The theoretical predictions calculated from Hudson (1981) and Chapman (2003) for P and S wave velocity of the three rocks with cracks fit the measured data well (as shown in Figs. 8, 9, and 10). The P wave velocity calculated from the theoretical model quantitatively fits the measured data in most directions for the three rocks with cracks. The theoretical predictions by Hudson's model are slightly higher than the measured data in the 0° direction when crack density is higher (shown in Fig. 10). Note that the P wave velocity in 0° direction is not the minimum one in Hudson's model, which is due to the assumption of isolated cracks in high-frequency limit in Hudson's model. The unrelaxed fluids enclosed in the cracks increase the stiffness of rocks when P wave propagates in the 0° direction. SH wave velocity predicted by Chapman's and Hudson's models fit the measured

data well; SV velocity predicted by Hudson's model is comparatively higher than Chapman's model prediction and the measured data. Chapman's model fits the P wave velocity data better than Hudson's model does, particularly in the 45° direction. P wave velocity predicted by Hudson's model in this direction is comparatively higher than Chapman's model prediction and the measured data. Both Hudson model and Chapman model accurately predict SH wave velocity. The SV velocities predicted by Hudson's model are apparently higher than the measured data and Chapman's model predictions.

The influence of crack density on P wave velocity is shown in Fig. 11. P wave velocity in 90° direction (parallel to crack planes) is not affected by cracks, but P wave velocity in 0° direction (orthogonal to crack planes) decreases significantly as the crack density increases. Comparatively, Chapman's model gives better prediction than Hudson's model. Figure 12a shows that the S wave velocity in 0° direction (propagation orthogonal to crack planes) decreases with the increasing crack density; both SH wave and SV wave velocity are significantly affected by cracks. Figure 12b shows that the S wave velocity in 90° direction (propagation parallel to crack planes) changes with the increasing crack density: $V_{SH}(90^\circ)$ is not affected by cracks, whereas $V_{SV}(90^\circ)$ significantly decreases when crack density increases. Both



◀Figure 6

Transmission waveforms of *P* and *S* wave signal in four samples. **a–d** Show *P* wave signal in #1, #2, #3, #4 samples respectively. **e–h** Show *S* wave signal in 1#, 2#, 3#, 4# samples respectively

Hudson's model and Chapman's model give good prediction for *S* wave velocity for propagation in 90° direction.

The influence of crack density on *P* wave anisotropy ε and *S* wave anisotropy γ is shown in Fig. 13. In this study, we compared measurement results for *P* and *S* wave anisotropy to theoretical predictions based on Hudson (1980, 1981) and Chapman (2003). As the properties of rocks and cracks have been given and elastic wave velocities shown in Figs. 7, 8, 9, and 10, these parameters are used to calculate the theoretical results on *P* and *S* wave anisotropy (as shown in Fig. 13). The theoretical prediction of *P* wave anisotropy from Chapman model is slightly lower than the measured value, while Hudson model gives much lower *P* wave anisotropy than measured data and Chapman model. In contrast, both Chapman model and Hudson model yield good predictions for *S* wave anisotropy. Overall, Chapman's poroelastic model provides more accurate predictions than Hudson's model. As shown in Fig. 13, both *P* and *S* wave anisotropy increase significantly with crack density. Shear wave anisotropy γ is comparatively a little more sensitive to crack density. Comparatively, this intrinsic anisotropy of blank rock is much smaller

than crack-induced anisotropy in three rocks with aligned cracks (as shown in Fig. 13). Overall, the strength of seismic anisotropy due to aligned cracks is proportional to crack density, as predicted by theoretical models (Chapman 2003; Crampin 1984; Hudson 1981). This provides an effective model for (1) determining the strength of crack development through extracting anisotropy from seismic or VSP data; and (2) helping geophysicists and reservoir engineers to obtain crack density information for crack detection and oil production. Nevertheless, the frequency effects (i.e. dispersion in fluid saturated cracked rocks) between the ultrasonic frequency range used in the lab (MHz) and the lower frequencies used in the field (i.e. well logging and seismic data) should be further researched. This study shows frequency-dependent model described by Chapman give more accuracy prediction than Hudson's model, but the measurement frequency (0.5 MHz) is still in the high-frequency range.

4. Discussion

The waveforms for both *P* and *S* wave show the effect of the elastic wave interaction in cracked samples. Because the wavelength of the propagating ultrasonic waves (4–7 mm) is comparable to the crack size (3 mm), the cracked samples cannot be considered as homogeneous and scattering effects are

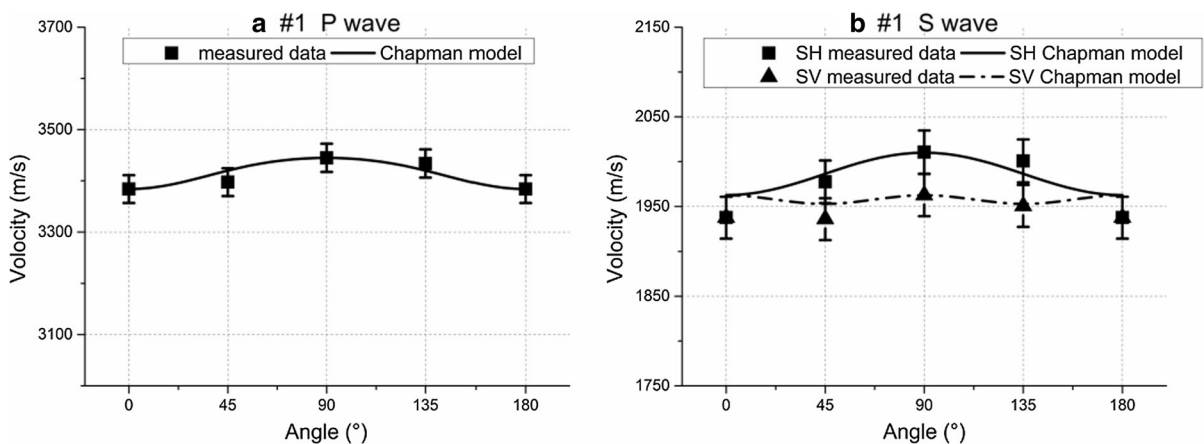


Figure 7

Measured velocity (black square) and theoretical predictions (curves) for #1 sample (blank sample). Based on the background matrix properties, Chapman model and Hudson model give the same theoretical curve. The figures show the theoretical models fit measured data

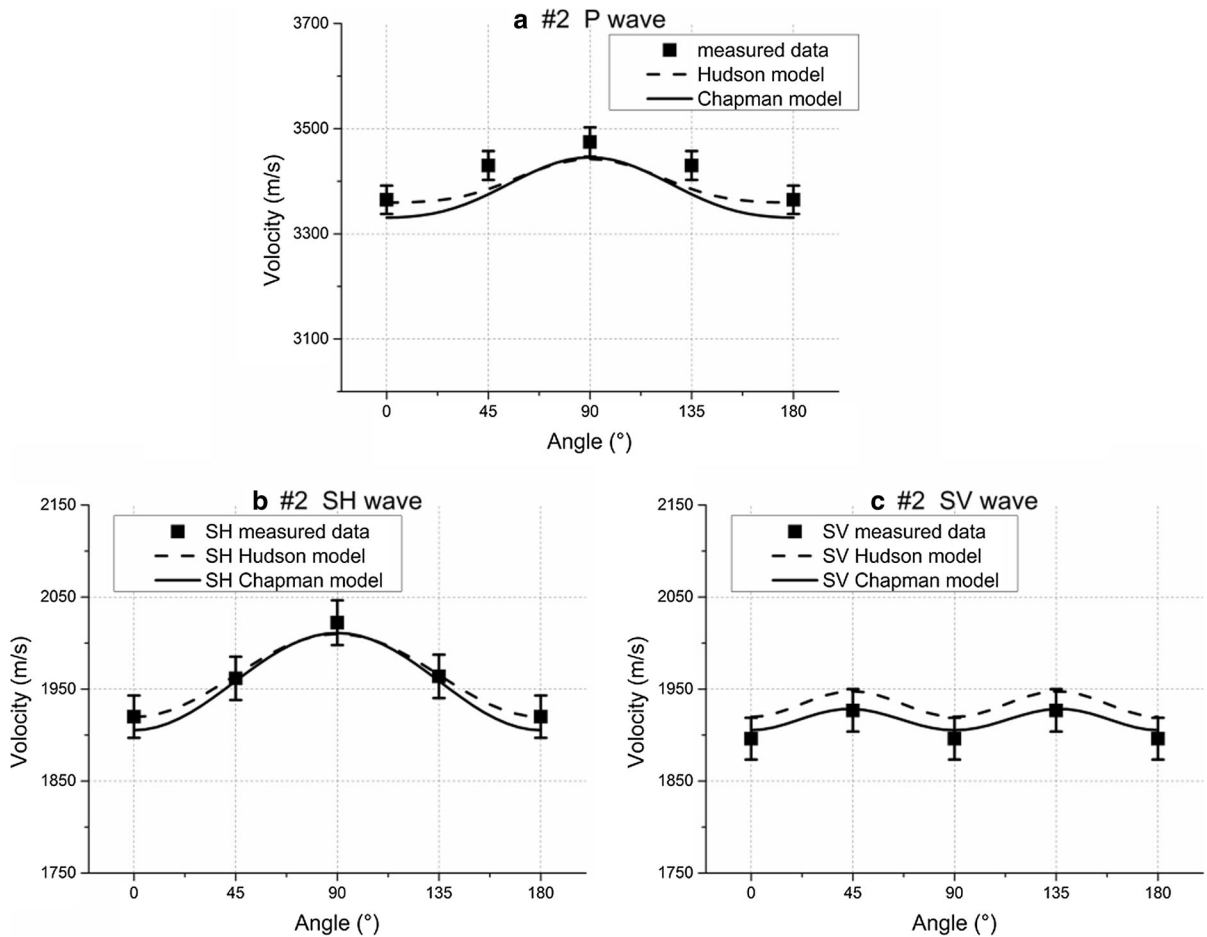


Figure 8

Measured velocity (*black square*) and theoretical predictions (*solid curves* for Chapman model, *dash curves* for Hudson model) for #2 sample (crack density is 0.0243)

expected. The scale of cracks in natural rocks varies from kilometers (large-scale fractures related to geological tectonic activity) to nanometers (small cracks in shales) (Barbier et al. 2012; De Keijzer et al. 2007; Stephenson et al. 2007). The evaluation of the effects of large-scale fractures is more critical for geophysical exploration and reservoir production because fluid accumulation and migration is mostly controlled by these features. In this case, the elastic wave propagation should be affected by scattering. For ultrasonic investigation in the laboratory and for well logging, cracked rocks present a heterogeneity that may introduce both dispersion and scattering. Thus the characterization of cracked rock is a complex task; further theoretical and experimental

research is required for describing cracked media with higher accuracy.

In Hudson's model, elastic stiffness for the second order has been observed to inconsistently increase with crack density beyond a crack density threshold value of 0.1 (Grechka and Kachanov 2006; Liu et al. 2000). In this study, the main purpose was to investigate the anisotropy change when crack density increases (the crack density of samples studied is 0.0243, 0.0486, 0.0729). Because the crack densities are still lower than that threshold value for Hudson's model, we expect that Hudson's model provide useful predictions for comparison purposes.

Chapman's model gives a more precise description of the elastic wave propagation in saturated

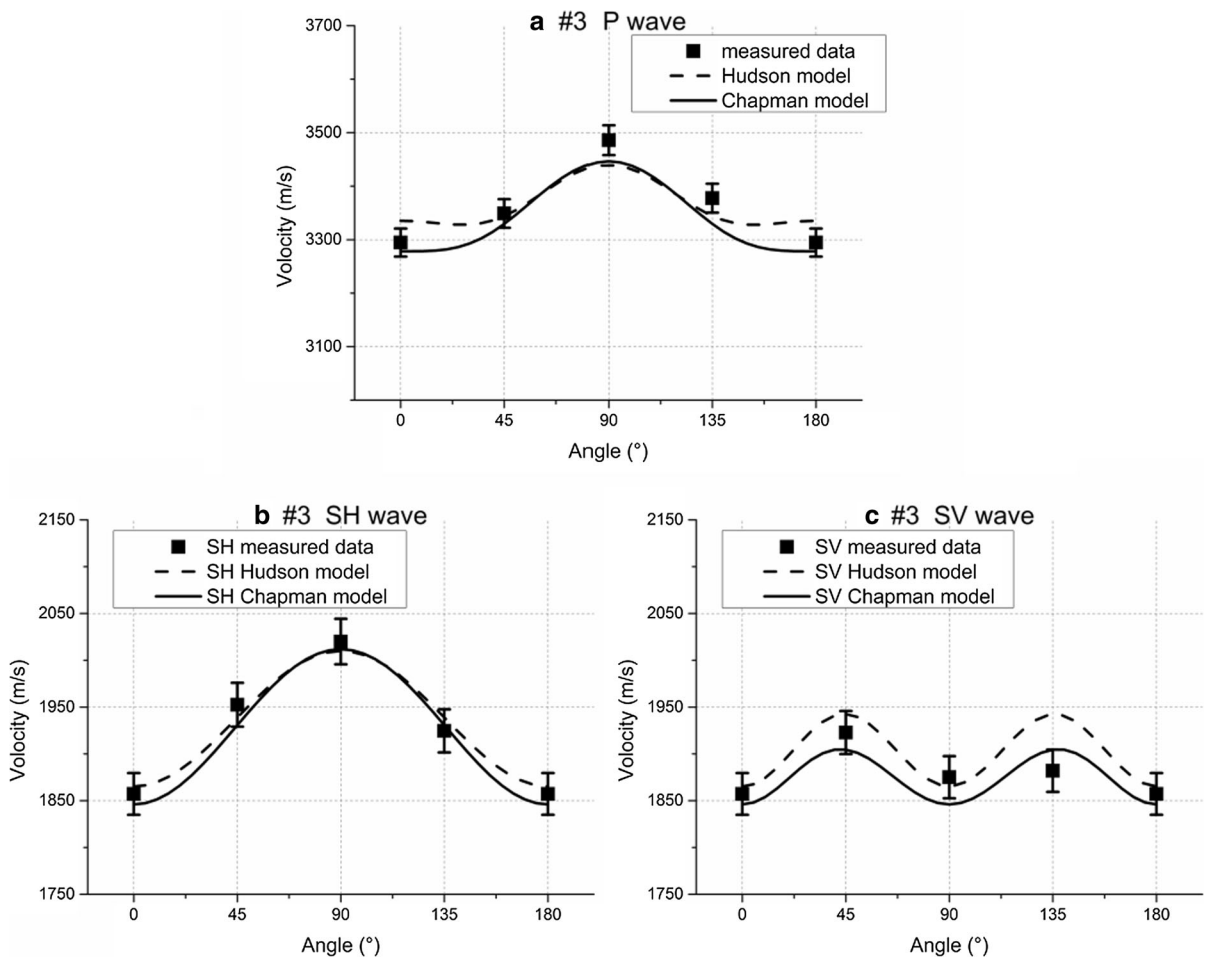


Figure 9

Measured velocity (*black square*) and theoretical predictions (*solid curves* for Chapman model, *dash curves* for Hudson model) for #3 sample (crack density is 0.0486)

cracked rocks. Because Hudson's model considers that fluid is isolated in pores and cracks, its use should be restricted to the high-frequency limit. In this limit, the elastic stiffness tensor components in the parallel and perpendicular directions are enhanced because of the unrelaxed fluid pressure. In contrast, Chapman's model takes into account both fluid interactions and frequency-dependent effects, that is, fluid flow between the cracks and the surrounding porous rock is controlled by the fluid mobility and by the frequency of the elastic wave. In the high-frequency range, fluid pressure has no time to relax and fluids remain enclosed in the cracks and pores. The effective elastic stiffness in this case is

similar to that predicted by Hudson's model. In the low-frequency range, local fluid pressure has enough time to relax and effective elastic stiffness appears lower in the direction perpendicular to the crack planes and higher in the parallel direction. In this case, elastic wave velocity in the perpendicular direction is lower compared to the high-frequency limit, while P anisotropy is higher. Figure 13 shows that the P wave anisotropy predicted by Hudson's model is much lower than measured. Over all, Chapman's model gives better results than Hudson's model. This indicates that the measurement results in this study are not in the high-frequency range assumed by Hudson's model. In this study, the

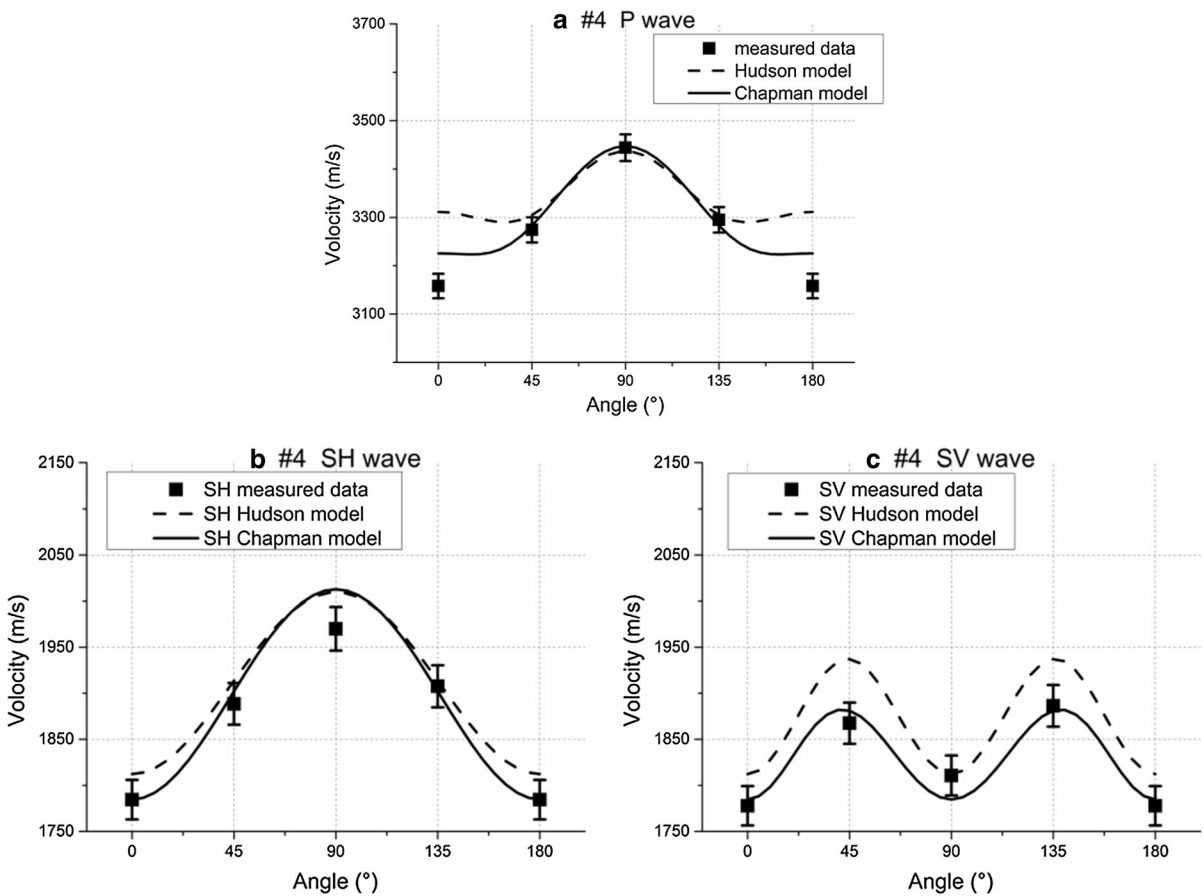


Figure 10

Measured velocity (*black square*) and theoretical predictions (*solid curves* for Chapman model, *dash curves* for Hudson model) for #4 sample (crack density is 0.0729)

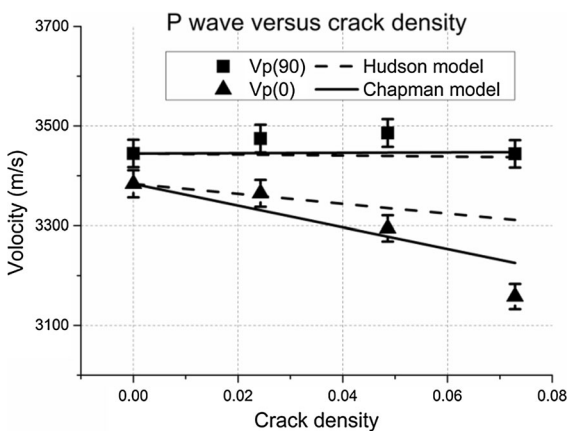


Figure 11

P wave velocity in both 0° direction and 90° direction. *Black square* is measured data in 90° direction, *black-up-pointing triangle* is measured data in 0° direction. *Solid line* is the Chapman's prediction, *dash line* is the Hudson's prediction

poroelastic model can provide better predictions for elastic constants of cracked porous rocks. Similar to Rathore et al. (1995), the results of this study indicate that the pores and fluids should be considered in theoretical models.

5. Conclusions

This study focuses on the dependence of seismic velocity and anisotropy on crack density, through observing P and S wave velocity and anisotropy in a set of synthetic rocks with controlled crack geometry. The new rock manufacturing process provides a method for constructing synthetic rocks similar to natural rocks: similar mineral composition, porous structure, and cementation. One blank rock and three

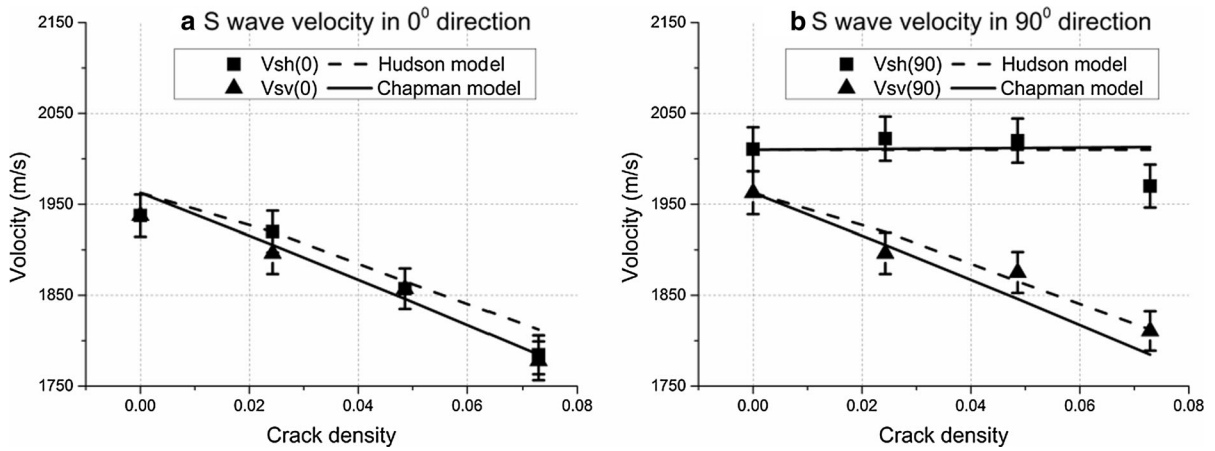


Figure 12

S wave velocity in both 0° direction (a) and 90° direction (b). Black square is measured data for SH wave velocity, black-up pointing triangle is measured data for SV wave velocity. Solid line is the Chapman’s prediction, dash line is the Hudson’s prediction

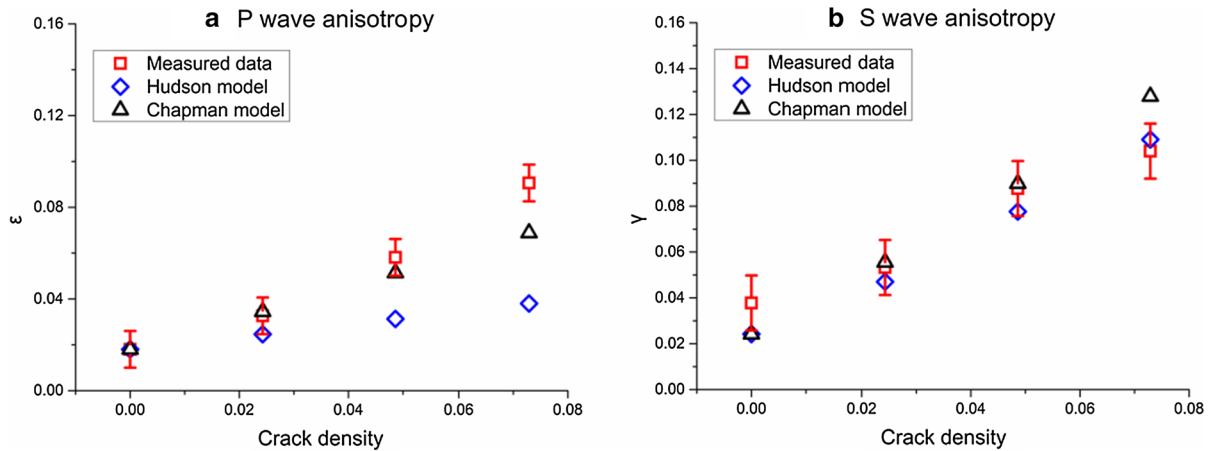


Figure 13

P and S wave anisotropy in synthetic rocks with controlled crack density. White square is measured data, white-up pointing triangle is Chapman model, open diamond is Hudson model

cracked rocks with different crack density have been used for laboratory ultrasonic measurements at 0.5 MHz while the rocks were saturated with water. The measurements show the influence of crack density on P and S wave velocities in different directions. The measured data are compared with the predictions of Chapman’s model and Hudson’s model and show that the theoretical predictions are in overall quantitative agreement with the model predictions for the three water-saturated cracked rocks with different crack densities. However, Chapman’s model more accurately fits the laboratory data. Moreover, the

comparison of theoretical predictions and measured data shows the effective medium has the capability for obtaining accurate crack density for cracked reservoir detection.

Acknowledgements

We thank Mark Chapman from the University of Edinburgh who provided sustained support during the entire research. Special thanks to David Booth from British Geological Survey for proofreading. This

research is supported by the National Natural Science Fund Projects (U1663203) and the National Natural Science Fund Projects (41474112).

Appendix

In the case of a material containing aligned or randomly orientated cracks, the overall elastic properties derived by Hudson contain the second order in the concentration. Both the single scattering formulae, which are correct to the first order in crack density ε_c , and crack–crack interactions, which are correct to the second order in crack density, are accounted. The model considered a plane wave propagating through the medium with cracks, but the pores in the background matrix are neglected.

The stiffness tensor of the medium contain cracks in the Hudson model is given as

$$C_{ij} = C_{ij}^0 + C_{ij}^1 + C_{ij}^2, \tag{4}$$

in which C_{ij} is the total stiffness tensor, C_{ij}^0 is the background, C_{ij}^1 , and C_{ij}^2 are the first- and second-order effects of the cracks:

$$C_{ij}^0 = \begin{bmatrix} \lambda + 2\mu & \lambda & \lambda & 0 & 0 & 0 \\ \lambda & \lambda + 2\mu & \lambda & 0 & 0 & 0 \\ \lambda & \lambda & \lambda + 2\mu & 0 & 0 & 0 \\ 0 & 0 & 0 & \mu & 0 & 0 \\ 0 & 0 & 0 & 0 & \mu & 0 \\ 0 & 0 & 0 & 0 & 0 & \mu \end{bmatrix}, \tag{5}$$

$$C_{ij}^1 = -\frac{\varepsilon_c}{\mu} \begin{bmatrix} \lambda^2 \bar{U}_{33} & \lambda^2 \bar{U}_{33} & \lambda(\lambda + 2\mu) \bar{U}_{33} & 0 & 0 & 0 \\ \lambda^2 \bar{U}_{33} & \lambda^2 \bar{U}_{33} & \lambda(\lambda + 2\mu) \bar{U}_{33} & 0 & 0 & 0 \\ \lambda(\lambda + 2\mu) \bar{U}_{33} & \lambda(\lambda + 2\mu) \bar{U}_{33} & \lambda(\lambda + 2\mu) \bar{U}_{33} & 0 & 0 & 0 \\ 0 & 0 & 0 & \mu^2 \bar{U}_{11} & 0 & 0 \\ 0 & 0 & 0 & 0 & \mu^2 \bar{U}_{11} & 0 \\ 0 & 0 & 0 & 0 & 0 & 0 \end{bmatrix}, \tag{6}$$

$$C_{ij}^2 = \frac{\varepsilon_c^2}{15} \begin{bmatrix} \frac{\lambda^2 q}{\lambda + 2\mu} \bar{U}_{33}^2 & \frac{\lambda^2 q}{\lambda + 2\mu} \bar{U}_{33}^2 & \lambda q \bar{U}_{33}^2 & 0 & 0 & 0 \\ \frac{\lambda^2 q}{\lambda + 2\mu} \bar{U}_{33}^2 & \frac{\lambda^2 q}{\lambda + 2\mu} \bar{U}_{33}^2 & \lambda q \bar{U}_{33}^2 & 0 & 0 & 0 \\ \lambda q \bar{U}_{33}^2 & \lambda q \bar{U}_{33}^2 & (\lambda + 2\mu) q \bar{U}_{33}^2 & 0 & 0 & 0 \\ 0 & 0 & 0 & \frac{2\mu(3\lambda + 8\mu)}{\lambda + 2\mu} \bar{U}_{11}^2 & 0 & 0 \\ 0 & 0 & 0 & 0 & \frac{2\mu(3\lambda + 8\mu)}{\lambda + 2\mu} \bar{U}_{11}^2 & 0 \\ 0 & 0 & 0 & 0 & 0 & 0 \end{bmatrix}. \tag{7}$$

in which $q = 15 \left(\frac{\lambda}{\mu}\right)^2 + 28 \left(\frac{\lambda}{\mu}\right) + 28$. In the case of water saturation,

$$\bar{U}_{11} = \frac{16}{3} \frac{\lambda + 2\mu}{3\lambda + 4\mu}, \quad \bar{U}_{33} = 0. \tag{8}$$

The Chapman’s model considers frequency-dependent seismic anisotropy in fractured rocks through knowledge of rock porosity, permeability, fracture density, and pore fluid properties. The model is based on fluid interactions at two scales: randomly aligned microcracks and aligned mesoscale fractures.

The stiffness tensor given by Chapman (2003) is

$$C_{ijkl}(\omega) = C_{ijkl}^0 - \phi_p C_{ijkl}^1 - \varepsilon_c C_{ijkl}^2 - \varepsilon_f C_{ijkl}^3, \tag{9}$$

where C_{ijkl}^0 is the isotropic background matrix of porous rock, C_{ijkl}^1 , C_{ijkl}^2 , and C_{ijkl}^3 are the contributions from pores, grain size cracks, and meso-scale fractures, respectively. ϕ_p is the porosity, ε_c is the crack density, and ε_f is the fracture density.

$$\varepsilon_c = \frac{N_c a_c^3}{V}; \quad \varepsilon_f = \frac{N_f a_f^3}{V}, \tag{10}$$

where N_c and N_f are the number of cracks and fractures in volume V , a_c and a_f are the radius of cracks and fractures, respectively. The model parameters are the functions of the elastic tensor (isotropic matrix λ and μ), fracture parameters, fluid properties, frequency, relaxation time τ_m of micro-scale pores and cracks, τ_f of meso-scale fractures.

In fact, fluid flow in the model takes place at two scales, micro-scale squirt flow in pores and cracks

and meso-scale flow in large fractures. The grain size local flow is related with the squirt flow relaxation time τ_m ; the flow at fracture scale is related with the larger relaxation time τ_f which depends on the fracture size. In the Chapman model, the relaxation time corresponding to the fractures, τ_f , is related to the fracture scale and micro-scale relaxation time τ_m as

$$\tau_f = \frac{a_f}{\zeta} \tau_m, \quad (11)$$

in which a_f is the fracture scale ζ is the grain size scale. and τ_m is given by

$$\tau_m = \frac{c_v \eta (1 + K_c)}{\sigma_c \kappa \zeta c_1}, \quad (12)$$

where η is the fluid viscosity, κ is the permeability, c_v is the volume of the individual cracks, K_c is the inverse of the crack space compressibility, $\sigma_c = \pi \mu r / [2(1 - \nu)]$ is the critical stress in which r is the aspect ratio of the cracks, ν is the Poisson's ratio of the isotropic rock matrix, and c_1 is the number of connections to other elements of the pore space.

Due to the calculation of the elastic constants following the interaction energy approach of Eshelby (1957), the original form of the Chapman model is limited to low porosity. To make the Chapman model more applicable to real data, a slightly modified version was described by Chapman et al. (2003) through introducing the λ^0 and μ^0 which were calculated from the measured V_p^0 and V_s^0 and density of the rock. Additionally, the model requires a $C_{ijkl}^0(A, M)$ term to be defined in a way that the fracture and pore corrections to velocities are applied at a specific frequency (w_0). Thus:

$$\begin{aligned} A &= \lambda^0 + \Phi_{c,p}(\lambda^0, \mu^0, f w_0); \\ M &= \mu^0 + \Phi_{c,p}(\lambda^0, \mu^0, w_0), \end{aligned} \quad (13)$$

where $\Phi_{c,p}$ is an elastic correction term that is proportional to ε_c and ε_f and with,

$$\lambda^0 = \rho (V_p^0)^2 - 2\mu^0; \quad \mu^0 = \rho (V_s^0)^2. \quad (14)$$

Then equation is written as follows:

$$\begin{aligned} C_{ijkl}(\omega) &= C_{ijkl}^0(A, M, w) - \phi_p C_{ijkl}^1(\lambda^0, \mu^0, w) \\ &\quad - \varepsilon_c C_{ijkl}^2(\lambda^0, \mu^0, w) - \varepsilon_f C_{ijkl}^3(\lambda^0, \mu^0, w). \end{aligned} \quad (15)$$

In this form, the correction for pores, microcracks, and fractures which describe the frequency dependence and anisotropy of the rock can be calculated with physical properties obtained from measured velocities. In the case of high porosity, the model is simplified by setting the microcrack density as zero. Therefore,

$$\begin{aligned} C_{ijkl}(\omega) &= C_{ijkl}^0(A, M, w) - \phi_p C_{ijkl}^1(\lambda^0, \mu^0, w) \\ &\quad - \varepsilon_f C_{ijkl}^3(\lambda^0, \mu^0, w). \end{aligned} \quad (16)$$

Based on the theoretical model, experimental data measured from synthetic samples are compared with theoretical results. The input parameters for theoretical calculation are the properties of the background matrix measured from the blank sample and fracture density. To model the anisotropy caused by fractures, the background anisotropy should be taken into account. A modified version of the Chapman model was generated by Chapman et al. (2003) to account for background layering anisotropy in the blank rock. Tillotson et al. (2011) used this simplified equation to model samples with background anisotropy: by replacing $C_{ijkl}^0(A, M, w)$ with $[C_{ijkl}^{\text{background}} + \Phi_{c,p} C_{ijkl}^1(\lambda^0, \mu^0, w, \text{water})]$; thus

$$\begin{aligned} C_{ijkl}(\omega) &= [C_{ijkl}^{\text{background}} + \Phi_{c,p} C_{ijkl}^1(\lambda^0, \mu^0, w, \text{water})] \\ &\quad - \phi_p C_{ijkl}^1(\lambda^0, \mu^0, w) - \varepsilon_f C_{ijkl}^3(\lambda^0, \mu^0, w), \end{aligned} \quad (17)$$

in which the background stiffness $C_{ijkl}^{\text{background}}$ is formed by the measured velocities ($V_p(0^\circ)$, $V_p(45^\circ)$, $V_p(90^\circ)$, $V_{sh}(0^\circ)$ and $V_{sh}(90^\circ)$) and density of the background rock.

REFERENCES

- Ass' Ad, J. M., Tatham, R. H., & McDonald, J. A. (1992). A physical model study of microcrack-induced anisotropy. *Geophysics*, 57, 1562–1570.
- Backus, G. E. (1962). Long-wave elastic anisotropy produced by horizontal layering. *Journal of Geophysical Research*, 67, 4427–4440.
- Barbier, M., Hamon, Y., Callot, J.-P., Floquet, M., & Daniel, J.-M. (2012). Sedimentary and diagenetic controls on the multiscale fracturing pattern of a carbonate reservoir: The Madison Formation (Sheep Mountain, Wyoming, USA). *Marine and Petroleum Geology*, 29, 50–67.

- Boness, N. L., & Zoback, M. D. (2004). Stress-induced seismic velocity anisotropy and physical properties in the SAFOD Pilot Hole in Parkfield, CA. *Geophysical Research Letters*, 31, L15S17.
- Cao, J., He, Z., Huang, D., & Li, Q. (2003). Seismic responses of fractured reservoirs by physical modeling. *Progress in Exploration Geophysics (in Chinese)*, 26, 88–93.
- Chapman, M. (2003). Frequency-dependent anisotropy due to meso-scale fractures in the presence of equant porosity. *Geophysical Prospecting*, 51, 369–379.
- Chapman, M., Maultzsch, S., Liu, E., & Li, X. Y. (2003). The effect of fluid saturation in an anisotropic multi-scale equant porosity model. *Journal of Applied Geophysics*, 54, 191–202.
- Chapman, M., Zatsepin, S. V., & Crampin, S. (2002). Derivation of a microstructural poroelastic model. *Geophysical Journal International*, 151, 427–451.
- Crampin, S. (1984). Effective anisotropic elastic constants for wave propagation through cracked solids. *Geophysical Journal of the Royal Astronomical Society*, 76, 135–145.
- De Keijzer, M., Hillgartner, H., Al Dhahab, S., & Rawnsley, K. (2007). A surface-subsurface study of reservoir-scale fracture heterogeneities in Cretaceous carbonates, North Oman. *Geological Society, London, Special Publications*, 270, 227–244.
- Ding, P., Di, B., Wang, D., Wei, J., & Li, X. (2014). P and S wave anisotropy in fractured media: Experimental research using synthetic samples. *Journal of Applied Geophysics*, 109, 1–6.
- Ding, P., Di, B., Wei, J., Di, X., Deng, Y., & Li, X. (2013). Laboratory measurements of P- and S-wave anisotropy in synthetic sandstones with controlled fracture density. *SEG Technical Program Expanded Abstracts*, 2013, 2979–2983.
- Eshelby, J. D. (1957). The determination of the elastic field of an ellipsoidal inclusion, and related problems. *Proceedings of the Royal Society of London. Series A. Mathematical and Physical Sciences*, 241, 376–396.
- Far, M. E., de Figueiredo, J. J. S., Stewart, R. R., Castagna, J. P., Han, D.-H., & Dyaar, N. (2014). Measurements of seismic anisotropy and fracture compliances in synthetic fractured media. *Geophysical Journal International*, 197, 1845–1857.
- Grechka, V., & Kachanov, M. (2006). Effective elasticity of fractured rocks: A snapshot of the work in progress. *Geophysics*, 71, W45–W58.
- Guéguen, Y., & Sarout, J. (2009). Crack-induced anisotropy in crustal rocks: Predicted dry and fluid-saturated Thomsen's parameters. *Physics of the Earth and Planetary Interiors*, 172, 116–124.
- Guéguen, Y., & Sarout, J. (2011). Characteristics of anisotropy and dispersion in cracked medium. *Tectonophysics*, 503, 165–172.
- Hall, S. A., Kendall, J. M., Maddock, J., & Fisher, Q. (2008). Crack density tensor inversion for analysis of changes in rock frame architecture. *Geophysical Journal International*, 173, 577–592.
- He, Z., Li, Y., Zhang, F., & Huang, D. (2001). Different effects of vertically oriented fracture system on seismic velocities and wave amplitude-Analyses of laboratory experimental results. *Computing Techniques for Geophysical and Geochemical Exploration*, 23, 1–5.
- Hudson, J. A. (1980). Overall properties of a cracked solid. *Mathematical Proceedings of the Cambridge Philosophical Society*, 88, 371–384.
- Hudson, J. A. (1981). Wave speeds and attenuation of elastic waves in material containing cracks. *Geophysical Journal of the Royal Astronomical Society*, 64, 133–150.
- Kuwahara, Y., Ito, H., & Kiguchi, T. (1991). Comparison between natural fractures and fracture parameters derived from VSP. *Geophysical Journal International*, 107, 475–483.
- Liu, E., Hudson, J. A., & Pointer, T. (2000). Equivalent medium representation of fractured rock. *Journal of Geophysical Research, A: Space Physics*, 105, 2981–3000.
- Lou, M., Shalev, E., & Malin, P. E. (1997). Shear-wave splitting and fracture alignments at the Northwest Geysers, California. *Geophysical Research Letters*, 24, 1895–1898.
- Mallick, S., & Frazer, L. N. (1991). Reflection/transmission coefficients and azimuthal anisotropy in marine seismic studies. *Geophysical Journal International*, 105, 241–252.
- Rathore, J. S., Fjaer, E., Holt, R. M., & Renlie, L. (1995). P- and S-wave anisotropy of a synthetic sandstone with controlled crack geometry. *Geophysical Prospecting*, 43, 711–728.
- Sarout, J., & Guéguen, Y. (2008a). Anisotropy of elastic wave velocities in deformed shales: Part 1—experimental results. *Geophysics*, 73, D75–D89.
- Sarout, J., & Guéguen, Y. (2008b). Anisotropy of elastic wave velocities in deformed shales: Part 2—modeling results. *Geophysics*, 73, D91–D103.
- Sarout, J., Molez, L., Guéguen, Y., & Hoteit, N. (2007). Shale dynamic properties and anisotropy under triaxial loading: Experimental and theoretical investigations. *Physics and Chemistry of the Earth, Parts A/B/C*, 32, 896–906.
- Schoenberg, M., & Sayers, C. M. (1995). Seismic anisotropy of fractured rock. *Geophysics*, 60, 204–211.
- Stephenson, B. J., Koopman, A., Hillgartner, H., McQuillan, H., Bourne, S., Noad, J. J., et al. (2007). Structural and stratigraphic controls on fold-related fracturing in the Zagros Mountains, Iran: Implications for reservoir development. *Geological Society, London, Special Publications*, 270, 1–21.
- Thomsen, L. (1986). Weak elastic anisotropy. *Geophysics*, 51, 1954–1966.
- Thomsen, L. (1995). Elastic anisotropy due to aligned cracks in porous rock. *Geophysical Prospecting*, 43, 805–829.
- Tillotson, P., Chapman, M., Best, A. I., Sothcott, J., McCann, C., Shangxu, W., et al. (2011). Observations of fluid-dependent shear-wave splitting in synthetic porous rocks with aligned penny-shaped fractures. *Geophysical Prospecting*, 59, 111–119.
- Tillotson, P., Sothcott, J., Best, A. I., Chapman, M., & Li, X.-Y. (2012). Experimental verification of the fracture density and shear-wave splitting relationship using synthetic silica cemented sandstones with a controlled fracture geometry. *Geophysical Prospecting*, 60, 516–525.
- Valcke, S. L. A., Casey, M., Lloyd, G. E., Kendall, J.-M., & Fisher, Q. J. (2006). Lattice preferred orientation and seismic anisotropy in sedimentary rocks. *Geophysical Journal International*, 166, 652–666.
- Varghese, A. V., Chapman, M., Li, X. Y., & Wang, Y. (2009). Observations of azimuthal variation of attenuation anisotropy in 3D VSPs. *SEG Technical Program Expanded Abstracts*, 2009, 4174–4178.
- Vernik, L., & Nur, A. (1992). Ultrasonic velocity and anisotropy of hydrocarbon source rocks. *Geophysics*, 57, 727–735.

- Wang, Y. (2011). Seismic anisotropy estimated from P-wave arrival times in crosshole measurements. *Geophysical Journal International*, *184*, 1311–1316.
- Wei, J.-X., Di, B.-R., & Ding, P.-B. (2013). Effect of crack aperture on P-wave velocity and dispersion. *Applied Geophysics*, *10*, 125–133.
- Zatsepin, S. V., & Crampin, S. (1997). Modelling the compliance of crustal rock—I. Response of shear-wave splitting to differential stress. *Geophysical Journal International*, *129*, 477–494.

(Received November 28, 2016, revised February 28, 2017, accepted March 6, 2017, Published online April 7, 2017)